water

MDPI

Article

Insight into the Influences of Blade Configuration on Internal Flow and Pressure Pulsation in High-Head Pump-Turbine: 9-Blade Versus 6+6 Long-Short-Blade Runners

Kai Zheng [1], Xijun Zhou [2], Yaopeng Li [3], Jiahao Lu [4], Wei Xiao [2] and Ruofu Xiao [4,*]

[1] State Grid Xinyuan Group Co., Ltd., Beijing 100000, China
[2] Pumped Storage Technology and Economy Research Institute of State Grid Xinyuan Company Ltd., Beijing 100761, China
[3] Jilin Dunhua Pumped Storage Co., Ltd., Beijing 132000, China
[4] College of Water Resources and Intelligent Engineering, China Agricultural University, Beijing 100083, China
* Correspondence: xrf@cau.edu.cn

Abstract

High-head reversible pump-turbines frequently suffer from hump-instability under pump-mode operation, and inherent performance trade-offs exist between pump-mode and turbine-mode characteristics for bidirectional operating requirements. The 6+6 long-short-blade runner is regarded as a promising candidate for mitigating pump-mode hump-instability. Taking a high-head pumped-storage pump-turbine as the research object, this study follows the above-mentioned engineering principle. A full-passage CFD model including volute, stay-ring, guide vanes, runner and draft-tube is established with the SST k-ω turbulence model. Numerical methods are validated against model-test external-characteristic data. Steady and unsteady simulations are carried out for the prototype 9-blade runner and the 6+6 long-short-blade runner. The results show that, under pump-mode operation, the 6+6 configuration shifts the hump-instability region toward lower mass-flow rates away from the unit's primary operating range. Short blades divide flow passages, suppress large-scale channel vortices within the hump zone, and alleviate flow asymmetry in the vaneless space. Nevertheless, local impingement and secondary-flow losses occur at long-short-blade junctions, and short-blade leading edges bear potential cavitation risk. This configuration only shifts the instability range rather than completely eliminating hump-instability. A typical 50% partial-load turbine-mode condition is selected for constraint-based verification. The 6+6 runner reduces pressure-pulsation amplitudes at draft-tube monitoring points by 25.52% and 19.83%, which suppresses occasional large-amplitude pressure fluctuations and improves signal periodic consistency. The novelty of this work lies in the quantitative revelation of such trade-off characteristics under the pump-priority-design philosophy for a 655 m high-head unit. It demonstrates that the 6+6 long-short-blade scheme is not a universal optimization measure.

Keywords: high-head pump-turbine; short-long blade(6+6); pressure fluctuation; flow field characteristics

Check for updates

Academic Editor: Vicente S. Fuertes-Miquel

Received: 29 September 2026
Revised: 11 October 2026
Accepted: 20 October 2026
Published: 26 October 2026

Copyright: © 2026 by the authors. Licensee MDPI, Basel, Switzerland. This article is an open access article distributed under the terms and conditions of the Creative Commons Attribution (CC BY) license.

1. Introduction

Driven by the "dual carbon" strategic goal, the construction pace of pumped storage power stations in China has continued to accelerate. As a core regulating power source in the new power system with multiple functions such as peak load regulation, valley

filling, frequency regulation, and phase regulation, high-head, large-capacity, and high-speed reversible pump-turbine have been widely applied in large-scale projects. With the continuous breakthrough of the design water head of the units and the further expansion of the operating condition range, high-head pump-turbine are facing severe hydraulic stability challenges [1–3]. The strong interference effect between rotor-stator, the narrow and elongated flow channel structure of the rotor, and the complex and variable operating conditions are prone to induce hydraulic instability phenomena such as pressure pulsation in the vaneless area, blade passage vortices, draft tube vortex bands, and S characteristics. This, in turn, leads to problems such as unit vibration, excessive swing, and component fatigue damage, seriously threatening the long-term safe and reliable operation of pumped storage units. It has become a key technical bottleneck restricting the development of high-head pumped storage equipment [4].

The runner is the core flow component of the pump-turbine for achieving bidirectional energy conversion between water energy and mechanical energy. The blade configuration directly determines the hydraulic efficiency, cavitation characteristics and flow stability of the unit, and is the core optimization target for improving internal flow and suppressing hydraulic instability phenomena [5–7]. A large amount of research has been conducted at home and abroad on the hydraulic optimization of the runner of high-head pump-turbine. Foreign research institutions, relying on model tests and CFD numerical simulation methods, have revealed the coupling amplification mechanism of cavitation in the draft tube, wake vortices of the runner, and pressure pulsations under non-optimal operating conditions, and proposed innovative design ideas such as variable geometry runners; at the same time, combined with artificial intelligence flow field reconstruction technology, they have achieved high-precision prediction of hydraulic performance, focusing on the control of the flow field and structural fatigue optimization under extreme part-load conditions. Domestic research and manufacturing units have completed the research and development of some 700-m-class ultra-high-head domestic pumped storage units. Through technical means such as double-curved blades, asymmetric guide vanes distribution, and segmented runner manufacturing, they have effectively improved the vibration and pressure pulsation levels of the units, marking that China's independent design and manufacturing of high-head pump-turbine has entered the international advanced ranks [8,9].

In the study of the stability of pump operation, the instability of the hump is a prominent challenge for pumped storage units operating in pumping mode at high water heads. Current research generally holds that the hump phenomenon is fundamentally attributed to the combined effects of vortex in the runner's blade passage, flow separation and rotational stall in the guide vane area under low-flow conditions. The flow channel blockage leads to non-monotonic changes in head, and the hump region is also accompanied by intense low-frequency pressure pulsations, directly threatening the operational safety of the unit in pumping mode. Zheng [10] et al. used the omega vortex to study the flow state of different guide vanes in the humped area based on the established criteria. The results showed that transitioning from the design condition to the humped area would cause unstable flow in the vaneless area, seriously threatening the operational stability of the pump-turbine. Zheng [11] et al. compared all the performance of the model tests under different conditions and analyzed the pressure pulsation characteristics. By analyzing the pressure pulsation characteristics of the pump-turbine under different flow rates in the humped area, the pressure pulsation laws of the pump-turbine operating in the humped area were revealed. Yang [12] et al. established a weakly compressible model using the Taylor equation to help study the flow mechanism inside the runner under humped conditions and obtained the results. In addition to the guide vanes, the hydraulic losses

caused by the unstable flow results inside the runner also greatly promoted the formation of the humped area.

The pressure pulsation under the operating conditions of the water turbine is another key issue that restricts the safe operation of the power generation system. The pressure pulsation under the operating conditions of the water turbine mainly consists of two types of sources: one is the high-frequency pulsation generated by the dynamic interference between the runner and the guide vanes, mainly at the blade passing frequency and its harmonics; the other is the low-frequency pulsation induced by the spiral vortex band of the draft tube under partial load, and these two types of pulsations are coupled with each other, which are important causes that trigger the vibration of the unit and the fatigue damage of the flow components. The model test results show that the amplitude of the pressure pulsation in the no-blade zone of high-head units can reach 10–20% of the head, and the vortex band of the draft tube will propagate upstream, further deteriorating the overall flow state. The blade configuration is an important means to regulate the characteristics of these two types of pulsations. Li [13] et al. studied the propagation characteristics of pressure pulsation in the water pump turbine under the power generation mode using the same-frequency tracking method. It was verified on the model water pump turbine test platform. The results showed that under different flow rates, the low-frequency pressure pulsation generated in the draft tube segment would propagate upwards along the spiral in the opposite direction of the vortex band. God [14] et al. investigated the influence of the split blade in the PAT system under two operating modes of pressure pulsation. They used DDES to analyze the internal flow structure and pressure pulsation of the 7+7 blade PAT. Yang [15] et al., in order to explore the relationship between pressure pulsation and the flow state caused by speed changes, conducted a three-dimensional numerical simulation to study the stable operation conditions of the water turbine and pump under different speeds. The results showed that when the pump operation is at the highest efficiency of the rated speed, the change in speed would lead to macroscopic parameter changes, deterioration of the flow state, and increase in pressure pulsation.

The configuration of short and long blades (long-short blades) is an important technical approach for regulating the flow in the runner. Many explorations have been carried out. This configuration relies on the alternating arrangement of short and long blades, re-dividing the blade passage and adjusting the distribution of blade loads. It has been widely applied in conventional mixed-flow turbines and can effectively suppress the blade passage vortices and improve pressure pulsation under certain operating conditions. Studies on related pumped storage units have shown that short blades can divide the pump operating flow passage and suppress large-scale blade passage vortices in the hump region; however, it has also been found that the improvement effects of short and long blades on the pump and turbine operating conditions are not synchronous, and there is a significant performance trade-off relationship. Liu [16] et al. conducted numerical and experimental studies on the pressure pulsation characteristics of turbine operating conditions for water turbines with three typical guide vane runner blade combinations: A: 20 GVs-9 RB, B: 20 GVs-11 RB, C: 16 GVs-5+5 RB. They analyzed the synergistic effect of long-short blades and guide vanes on pressure pulsation, and emphasized the role of RSI. He [17] et al. combined numerical simulation, entropy production analysis, and vortex transport equation analysis to study the transient flow characteristics in the hump region of the pump water turbine with long-short blades. The results show that the rotational stagnation originates from the flow separation within guide-vane passages. This pressure propagates in a circumferential direction through the interaction between vortex structures, starting from the reverse flow and sudden pressure gradient. Wei [18] et al. conducted a comprehensive and systematic analysis of the erosion characteristics and

potential mechanisms of high-head Francis water turbines with long-short blades under various operating conditions. The results show that both the main blades and the long-short blades have experienced significant erosion, which is highly consistent with the field observation results. In contrast, the erosion degree of the guide vanes is relatively light and mainly concentrated at the leading edge. However, most existing investigations on long-short-blade configurations are inherited from conventional Francis-turbine research or focus merely on either pump-mode or turbine-mode separately. For high-head pump-turbines, few studies have quantitatively compared prototype 9-blade and 6+6 long-short-blade runners following the industrial-applied principle of pump-mode-priority design with turbine-mode constraint verification. The bidirectional performance trade-offs brought by splitter-blade geometry remain insufficiently quantified, which constitutes a clear research gap for reversible runner hydraulic design and motivates the present work.

This paper takes the high-head pumping water turbine with a rated head of 655 m as the research object. Based on the full-flow CFD numerical simulation platform that has been verified by the original model test data, typical operating conditions of the pump and turbine are selected to conduct steady-state and unsteady numerical calculations of the prototype 9-blade runner and the 6+6 long-short blade runner [19,20]. Comparative analysis is carried out on the hump characteristics of the pump, the internal flow, and the pressure pulsation characteristics of the runner and draft tube of the turbine in the two blade configurations; based on the unsteady calculation results, the time-domain and frequency-domain characteristics of the pressure pulsation are obtained, revealing the mechanism of the effect of the long-short blade configuration on the pressure pulsation of the turbine working conditions of the high-head pumping water turbine; clarifying the advantages and limitations of the 6+6 long-short blade scheme, in order to provide theoretical references and technical support for the selection of runner blade configurations and hydraulic optimization design of reversible pumping water turbines with high head [21–23].

2. Numerical Governing Equations and Turbulence Model

The internal flow of the pump-turbine is a three-dimensional, incompressible, viscous turbulent flow. The flow characteristics are described by the continuity equation and the Navier-Stokes (N-S) momentum equation. The N-S equations represent the balance relationship among the momentum changes of fluid particles, the pressure of the flow field, the viscous dissipation force, and the mass force. The expressions in Cartesian coordinate system are given by Equations (1) and (2):

$$\frac{\partial \rho}{\partial t} + \frac{\partial (\rho v_x)}{\partial x} + \frac{\partial (\rho v_y)}{\partial y} + \frac{\partial (\rho v_z)}{\partial z} = 0 \tag{1}$$

where, ρ is density of the fluid medium; t is time; v_x, v_y and v_z are the components of velocity vector in the X, Y and Z directions respectively.

$$\frac{\partial (\rho v)}{\partial t} + (\rho v \cdot \nabla) v = -\nabla p + \mu \nabla^2 v + \rho f \tag{2}$$

where, μ is dynamic viscosity coefficient of fluid, v is velocity vector, $\bigtriangledown$ is nabla operator, and f is stress vector.

The three-dimensional turbulent flow calculation theory within the pump turbine is mainly based on the three-dimensional Navier-Stokes average equation turbulent flow theory. This theory mainly includes the Reynolds stress model and the vortex viscosity model. According to relevant literature, the SST k-ω standard model can be used to predict the performance of the pump and has been widely applied in engineering. In this study,

the SST k-ω turbulent flow model is selected, and the equations for the turbulent kinetic energy k and the specific turbulent dissipation rate ω are as shown in the formula:

$$\frac{\partial(\rho k)}{\partial t} + \frac{\partial(\rho u_i k)}{x_i} = P - \frac{\rho k^{3/2}}{l_{k-w}} + \frac{\partial(\rho k)}{\partial x_i}\left[(\mu + \sigma_k \mu_i)\frac{\partial k}{\partial x_i}\right] \quad (3)$$

$$\frac{\partial(\rho\omega)}{\partial t} + \frac{\partial(\rho u_i \omega)}{x_i} = C_\omega P - \beta\rho\omega^2 + \frac{\partial}{\partial x_i}\left[(\mu_l + \sigma_\omega \mu_t)\frac{\partial\omega}{\partial x_i}\right] + 2(1 - F_1)\frac{\rho\sigma_{\omega 2}}{\omega}\frac{\partial k}{\partial x_i}\frac{\partial\omega}{\partial x_i} \quad (4)$$

where ρ is the fluid density, P is the turbulence generation term, μ is the dynamic viscosity, μ_t is the eddy viscosity coefficient, σ is the model constant, C_ω is the coefficient of turbulent dissipation term, F_1 is the blending equation, k-ω is the scale of turbulence. In the term $\rho k^{3/2}/l_{k\text{-}\omega}$, the expression for the turbulence scale $l_{k\text{-}\omega}$ is given by Equation (5):

$$l_{k-\omega} = k^{1/2}\beta_k\omega \quad (5)$$

3. Computational Setup

3.1. Computational Geometry

This paper takes a 655 m rated head reversible pump-turbine model as the research object. The full flow passage computational domain completely encompasses the volute, stay vanes of the seat ring, guide vanes, runner, and draft tube, which are the five major flow passage components. Two sets of runner geometries are constructed: a 9-blade runner, and a 6+6 alternating short and long blade runner. The full flow passage fluid domain model is shown in Figure 1 and Table 1.

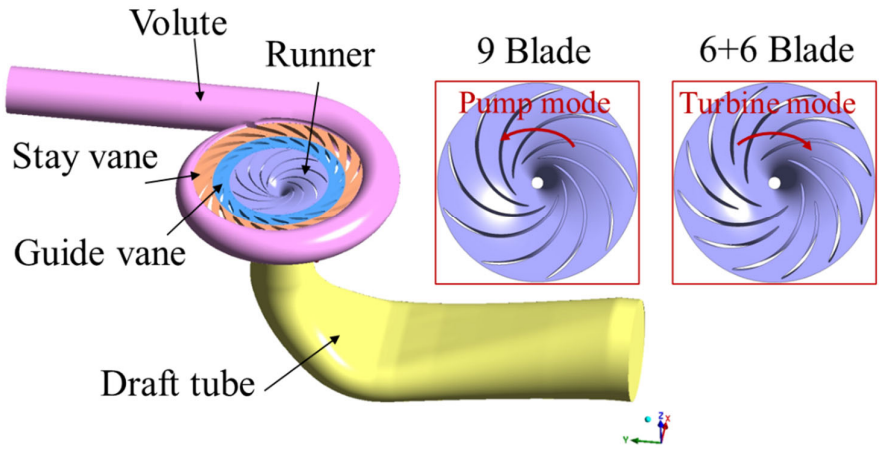

Figure 1. Fluid domain model of pump turbine.

Table 1. Main parameters of pump-turbine.

Parameter	Symbol	Value	Unit
Inlet diameter of runner	D_1	0.553	m
Outlet diameter of runner	D_2	0.252	m
Rated output	P	357	MW
Rotating speed	n_s	1150	r/min
Rated head	H_r	655	m

3.2. Mesh Generation and Mesh Independence Verification

A mixed-grid strategy was adopted for the entire flow channel meshing: the volute was meshed with tetrahedral grids; the stay vanes, guide vanes, runner, and draft tube were meshed with hexahedral structured grids. For the key areas with large flow gradients,

local mesh densification was carried out, and the value of y+ was strictly controlled, with its range being between 10 and 300, in order to ensure the accuracy of the boundary layer solution. The overall mesh is shown in Figure 2.

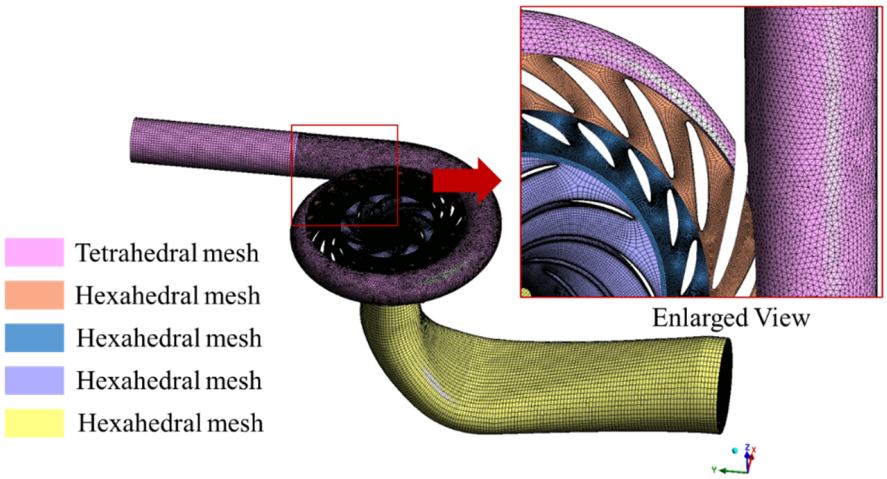

Figure 2. Schematic of full-passage mesh for the pump-turbine.

Using the head at a design flow rate of Q = 0.233 m^3/s as the evaluation parameter, convergence analysis was conducted for three sets of grids: 1.262 million, 2.982 million, 4.441 million cells. The refinement factors r_{32} and r_{21} were 1.3321 and 1.3189 respectively. Based on Richardson extrapolation, GCI_{32} = 0.183% and GCI_{21} = 0.0224% (Figure 3 and Table 2). Both sets of grids had convergence indices less than 0.5%, so considering both discretization error and computational cost, the subsequent calculation adopted the grid scheme of 298 ten thousand grids.

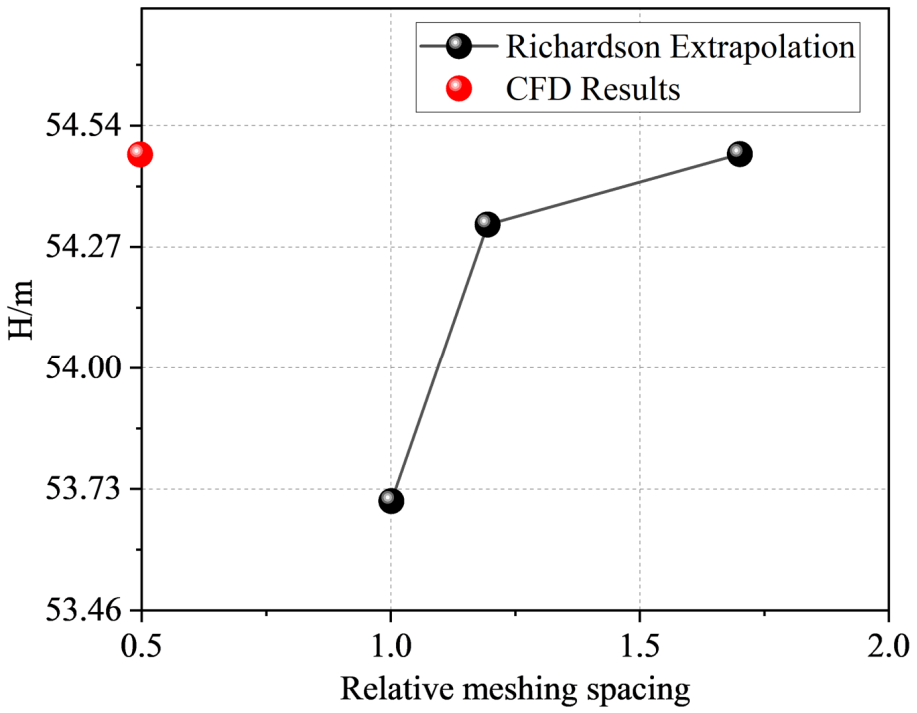

Figure 3. Grid independence verification results.

Table 2. Number of grid divisions in the fluid domain.

Overcurrent Component	Grid Format	Grid Number
Volute	Tetrahedral mesh	181,082
Runner	Hexahedral mesh	428,158
Guide Vane	Hexahedral mesh	835,040
Stay Vane	Hexahedral mesh	1,387,812
Draft Tube	Hexahedral mesh	149,760
Total	Hybrid mesh	2,981,852

3.3. Boundary Conditions

Following the principle of designing based on the pump working condition and verifying the turbine working condition, the calculation is divided into two parts: the pump working condition and the turbine working condition. The fluid medium is set as normal temperature clear water with a density of 998.2 kg/m^3. For pump-mode, fluid enters the computational domain from the draft-tube inlet, and mass-flow-rate inlet boundaries are specified for different operating points, and the inlet mass flow corresponding to different working conditions is given. The static pressure outlet is set at the volute outlet, corresponding to the outlet static pressure of different head working conditions. All solid surfaces are set as non-slip adiabatic surfaces. The steady calculation adopts the frozen rotor (Frozen-Rotor) interface to handle the data transfer between the stationary and rotating parts; the unsteady pressure pulsation calculation adopts the transient rotor-stator (Transient-Rotor-Stator) interface to capture the dynamic interference effect between the rotor and the guide vanes; the spatial discretization uses the first-order upwind scheme, and the turbulence numerical scheme uses the first-order scheme. The steady-state calculation iterates 1000 steps, and the unsteady calculation iterates once every 10 steps, with a total of 10 cycles, a time step of 5.55556×10^{-4} s, and an RMS residual convergence target of 1×10^{-5}. Pressure monitoring points are arranged in the vaneless area and the draft tube to extract the time-domain pressure pulsation signals, and subsequent FFT spectral analysis is carried out. For turbine-mode, rotational direction and inlet/outlet boundaries are reversed accordingly.

3.4. Numerical Model Validation

To confirm the reliability of the CFD numerical model in this paper, the simulation results will be compared with the test data from the high-head pump turbine model test rig. The model test rig is shown in Figure 4. The test rig has a closed-loop hydraulic circuit, equipped with a torque and speed measurement system, high-precision flowmeter, and pressure sensor, meeting the IEC standards for pump turbine model tests.

The external characteristic curves of head-flow and efficiency-flow obtained through simulation under the pump operating conditions were compared with the measured data from the model test. The results are shown in Figure 5. It can be seen that the overall change trends of head and efficiency with flow obtained by CFD simulation are highly consistent with the test results; the calculation error near the optimal operating condition is less than 5%, meeting the engineering accuracy requirements of CFD simulation for rotating machinery. In conclusion, the numerical model and grid scheme established in this paper are reliable and can be used for the subsequent comparison analysis of the internal flow field, hydraulic performance and pressure pulsation of the 9-blade and 6+6 short and long blade runner.



Figure 4. Pump-turbine model test rig.

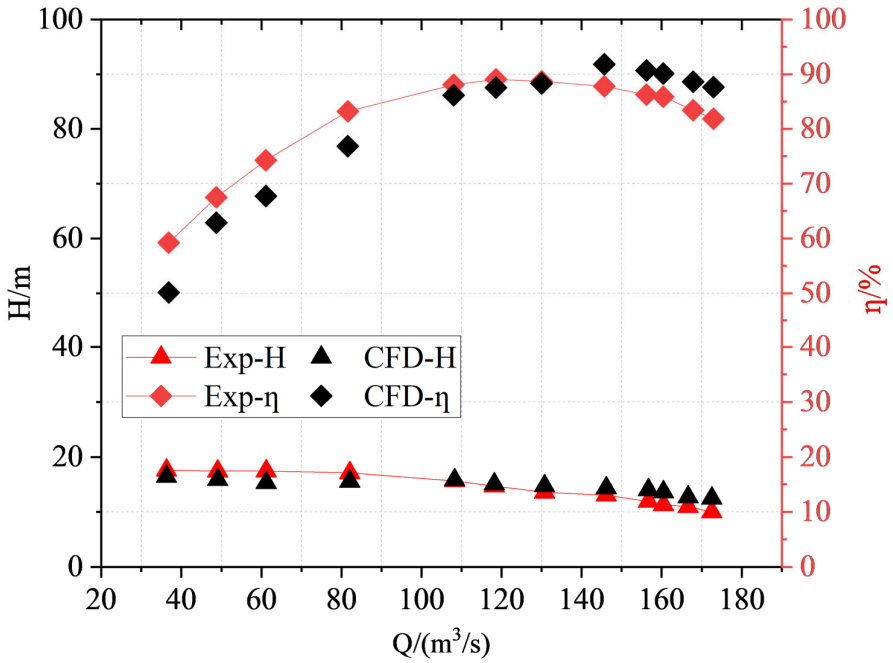

Figure 5. Comparison of pump-mode external characteristics between CFD simulation and model test.

4. Results and Analysis

4.1. Hydraulic Performance Comparison (Pump Mode)

The external operating characteristics of the 9-blade runner pump show a distinct non-monotonic variation in head in the low-flow range. There is partial overlap between the sensitive working area of the hump and the actual operating range of the unit. When the unit operates under variable conditions within this range, the uniformity of the internal flow in the runner significantly deteriorates, and the flow mismatch phenomenon intensifies, which adversely affects the stability of the pumping operation. To address this issue, the 6+6 long and short blades runner reconfigures the distribution of the blade passage channels and optimizes the load distribution of the blades, changing the energy diffusion and momentum exchange processes within the runner, thereby regulating the generation conditions and evolution path of the hump instability.

Figure 6 shows the comparison curve of mass flow rate and head for the 9-blade runner and the 6+6 long-short blade runner pump operation models. It can be seen that the 6+6 long-short blade scheme shifts the hump-instability zone as a whole towards the low-flow side, moving the originally unstable area close to the normal operating range of the unit away from the actual working range. This effectively reduces the risk of the unit entering the hump-instability zone during normal load variation regulation, and demonstrates superior hydraulic stability characteristics in terms of operational safety.

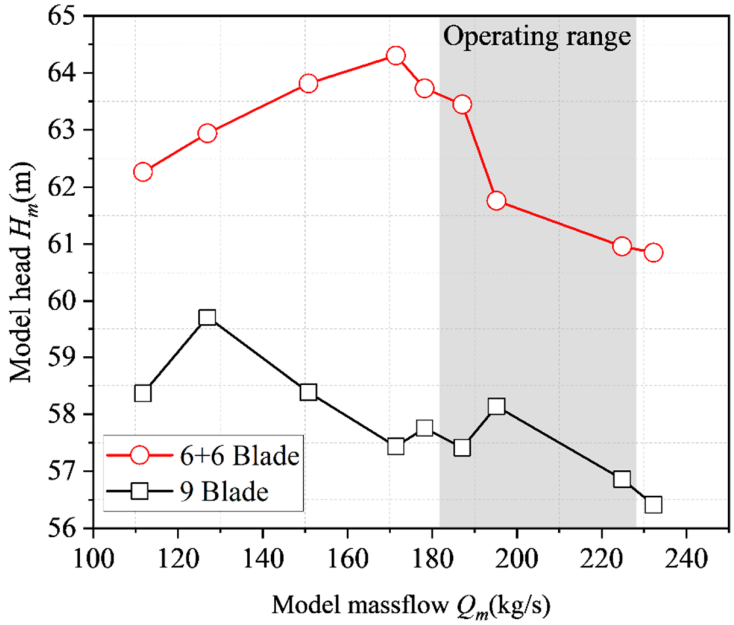

Figure 6. Comparison of hump characteristics between 9-blade and 6+6 blade configurations (guide vane opening = 14°).

However, the external characteristic curve also reveals that the 6+6 configuration, while achieving migration of the hump-instability regime, exhibits a more rapid head drop under high-flow conditions under high-flow conditions, indicating a performance trade-off. Therefore, it is necessary to combine the external characteristics and cross-sectional flow fields of typical working conditions to further reveal the intrinsic mechanism of the 6+6 runner in terms of the formation of the peak, the evolution of the flow structure, and the regulation of stability.

4.2. Steady Flow-Field Characteristics Comparison (Pump Mode)

Selecting multiple typical flow conditions in the high-flow and humped critical zone, the velocity streamlines and pressure contour diagrams of the two sets of runner sections were compared. The results are shown in Figure 7. Under the high-flow condition, the internal flow of both sets of runner channels was overall smooth, and the recirculation and flow separation phenomena were weak. As the flow gradually decreased, the reverse pressure gradient in the runner channels continued to increase, and the boundary layer on the suction surface of the blades separated, thereby generating a large-scale runner channel vortex structure.

For the 9-blade runner, in the humped low-flow condition, the blade passage vortices occupy a large portion of the flow passage cross-sectional area, causing significant flow passage blockage; the vortex structure further spreads to the vaneless area, inducing large-scale circumferential asymmetric flow in the vaneless area. The 6+6 long and short blade runner divides the original long blade flow passage with the short blades, achieving redistribution of blade loads and effectively suppressing the spatial scale and expansion

degree of the blade passage vortices. The asymmetric characteristics of the flow in the vaneless area are alleviated, and this flow field pattern is consistent with the phenomenon of the humped zone offset in the external characteristics. However, the interface position of the long and short blades will cause local fluid impact and secondary flow, forming local high-loss areas; a local low-pressure zone appears at the leading edge of the short blade, bringing potential cavitation risks, which is a design weakness that needs to be addressed for this configuration.

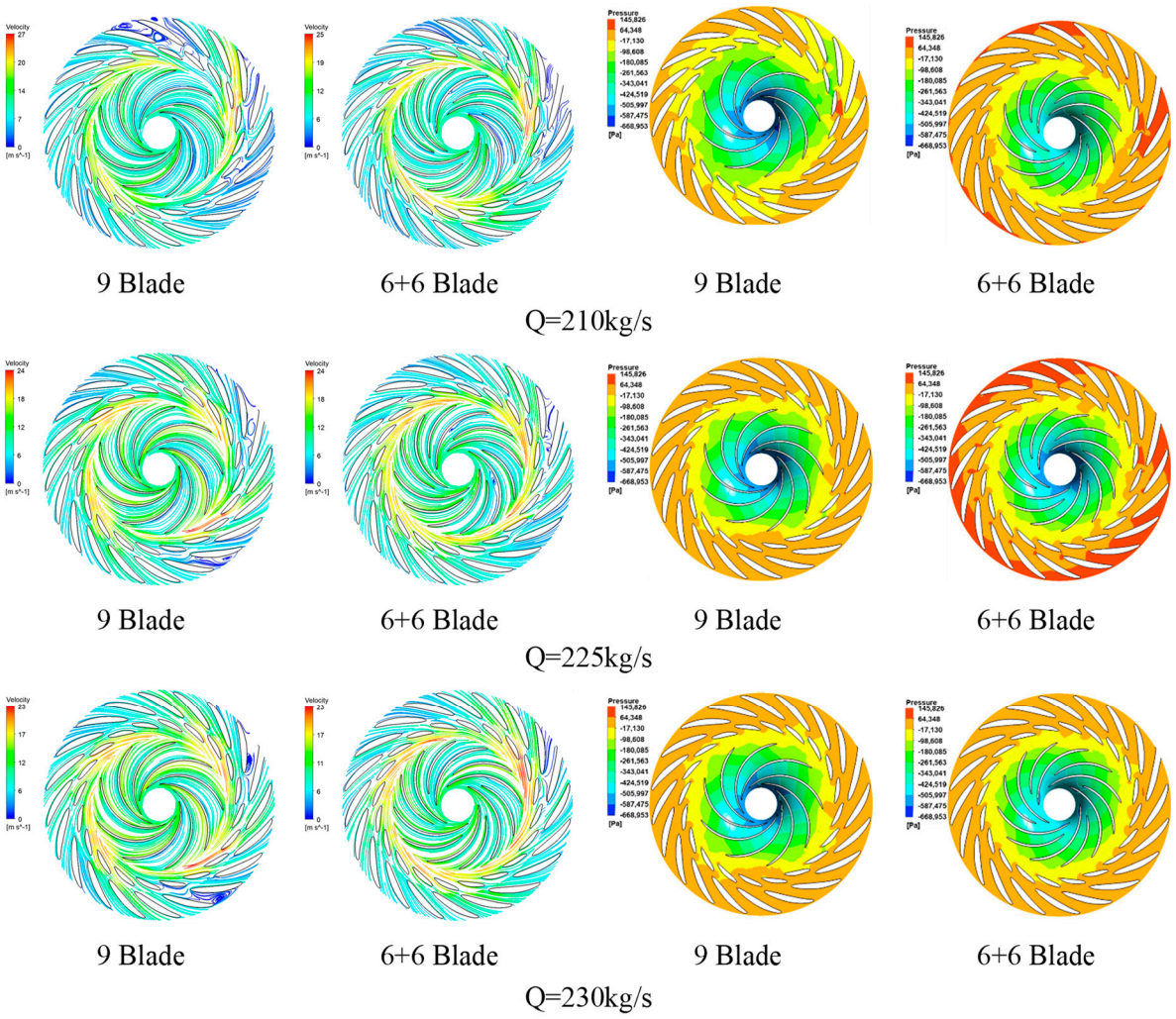

Figure 7. Comparison of internal flow patterns between the 9-blade and 6+6-blade configurations.

Even with the 6+6 configuration of long and short blades, when the flow rate further decreases to an extremely low level, significant flow separation will occur in both rotors. This configuration merely shifts the hump-instability regime toward lower flow rates rather than completely eliminating hump-instability.

4.3. Unsteady Flow and Pressure Pulsation Characteristics (Turbine Mode)

For reversible pump-turbines, the optimization of the runner structure not only affects the performance of the pump under normal conditions, but also alters the unsteady flow characteristics such as the wake at the outlet of the turbine runner, dynamic interaction between the rotor and stator, and rotational instability under the turbine operating conditions. Therefore, when evaluating the comprehensive performance of the optimization scheme, it is necessary to further examine the pressure pulsation response pattern under the turbine operating conditions.

Pressure pulsation is an important parameter reflecting the intensity of unsteady flow within the unit. Its generation is mainly closely related to the rotation of the runner, the interaction between the rotor and stator, and the evolution of local flow structures. Strong pressure pulsation not only increases the vibration and noise levels of the unit, but also may have adverse effects on the fatigue life of blades, guide vanes, and related flow components. Therefore, comparing and analyzing the pressure pulsation characteristics of different runner designs under typical turbine operating conditions is of great significance for evaluating the operational stability of the unit.

Therefore, this paper selects typical monitoring points in the vaneless area, the guide vane area, and the draft tube. Their spatial positions are shown in Figure 8 below. The spectral analysis of the pressure pulsation signals of the prototype runner and the optimized runner under the working conditions of the turbine is carried out, and the peak amplitudes of the pressure pulsation and the distribution patterns of the main characteristic frequencies of each scheme are compared in detail to reveal the influence of the runner structure optimization on the unsteady flow characteristics of the unit.

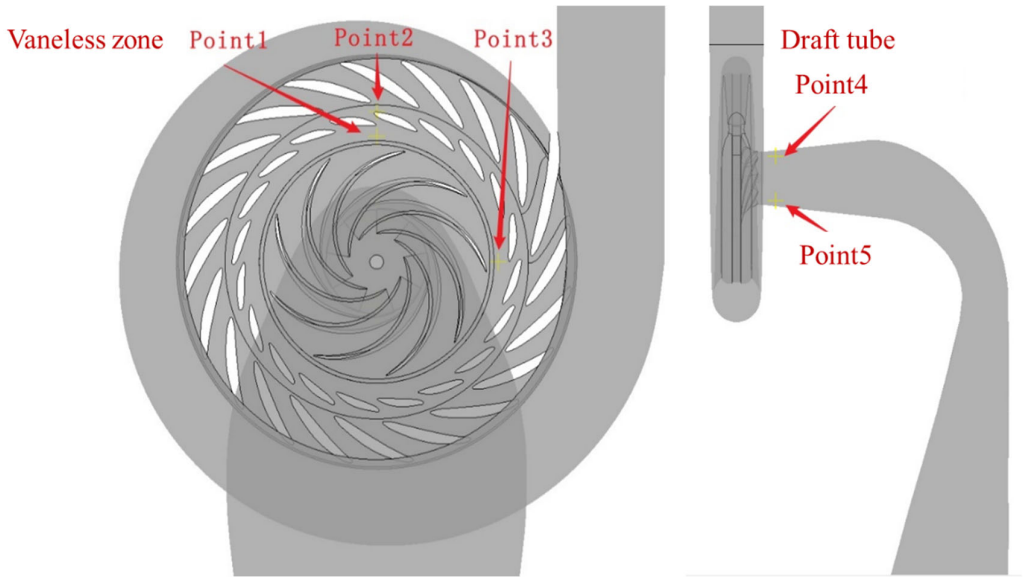

Figure 8. Schematic layout of pressure-pulsation monitoring points.

The pressure pulsation analysis was conducted for the model conversion condition corresponding to the rated water head of the prototype head and 50% output. The calculation parameters are listed in Table 3. This condition represents a typical partial load regulation load, deviating from the optimal efficiency point. Compared to the optimal condition, the uniformity of the flow field at the turbine outlet decreases under partial load, the trailing effect, residual vortices, and the interaction between the stationary and rotating parts are amplified, and the pressure pulsation phenomenon becomes more prominent. It is highly sensitive to the differences in turbine configuration and is suitable for verifying the unsteady flow performance of the two sets of turbines.

Figure 9 presents the time-domain and three-dimensional spectral results of the normalized pressure pulsations at each measurement point in the vaneless area and draft tube of the 9-blade runner. At measurement points P4 and P5 in the draft tube, prominent low-frequency main peaks occur near 0.4 fn, indicating that there is a strong large-scale unsteady flow inside the draft tube. This low-frequency pulsation is closely related to the physical mechanisms such as the draft tube rotating vortex structure, vortex band precession effect, and flow separation.

Table 3. Hydraulic turbine operating pressure pulsation calculation condition parameters.

Parameter Name	Symbol	Value
Prototype head (m)	H_p	655
Actual power output (MW)	P_p	177.28
Unit speed (-)	n_{QE}	38.87
Unit flow rate (L/s)	Q_{QE}	317.5
Guide vane opening (°)	a_0	10.04
Model speed (rpm)	n_M	1197
Model head (m)	H_M	60.25
Model flow rate (L/s)	Q_M	156.48

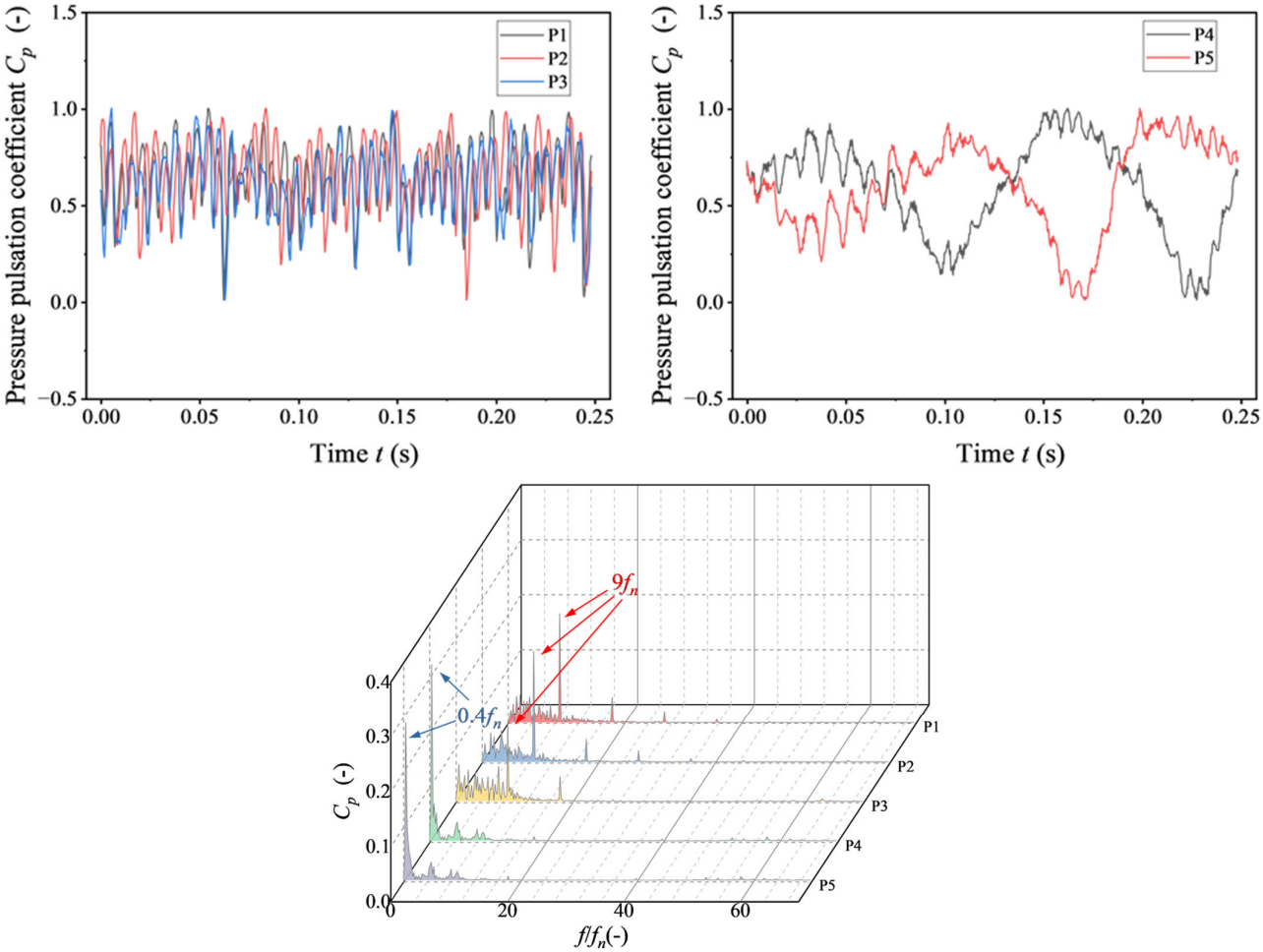

Figure 9. 9-blade runner pressure pulsation time-frequency domain diagram.

From the time-frequency domain results of all measurement points of the 9-blade runner, it can be observed that this runner exhibits two distinctly different types of unsteady pressure response characteristics under some partial load conditions of the turbine: The pressure pulsation energy in the vaneless area mainly concentrates at the frequency of the 9 fn blade passage and its various harmonic frequencies, indicating that the periodic sweeping of the runner blades, the trailing edge of the runner outlet, and the dynamic and static interference of the guide vanes are the dominant causes inducing the pressure fluctuations in the vaneless area; In the draft tube area, the 0.4 fn low-frequency pulsation is dominant, reflecting the circumferential non-uniform flow at the runner outlet and the residual vorticity transmitted downstream, thereby inducing large-scale unsteady flow in the draft tube. At the same time, the pulsation amplitudes and frequency components at

different circumferential positions of the monitoring points show significant differences, proving that the outlet flow field of the 9-blade runner has a remarkable circumferential non-uniformity characteristic.

The 6+6 long-short blade configuration does not simply increase the total number of blades. Instead, it reconfigures the topology of the runner's blade passage by alternately arranging long and short blades, achieving a redistribution of blade loads: The long blades undertake the main energy conversion task, while the short blades play a role in guiding the internal flow within the blade passage and sharing some of the load. This is done to optimize the flow field organization of the blade passage and improve the uniformity of the speed and pressure distribution at the runner outlet. The design intention of this configuration is to, while ensuring the core energy performance and safety margin of the unit, weaken the pressure pulsation in the vaneless area caused by the periodic sweeping of the blades and dynamic interaction between the rotor and stator, and by improving the flow state at the runner outlet, suppress the development of low-frequency unsteady flow in the draft tube.

To quantitatively evaluate the regulatory effect of this configuration on pressure pulsation, the calculation adopted the same working conditions, monitoring point layout, and post-processing procedures as the prototype 9-blade runner. As can be seen from the time-frequency domain results in Figure 10, the dominant frequency of pressure pulsation in the 6+6 long-short blade runner has significantly changed. New characteristic frequencies such as 1 fn, 6 fn, and 12 fn appear in the spectrum. This phenomenon directly results from the change in the distribution of blade numbers caused by the alternating arrangement of long and short blades.

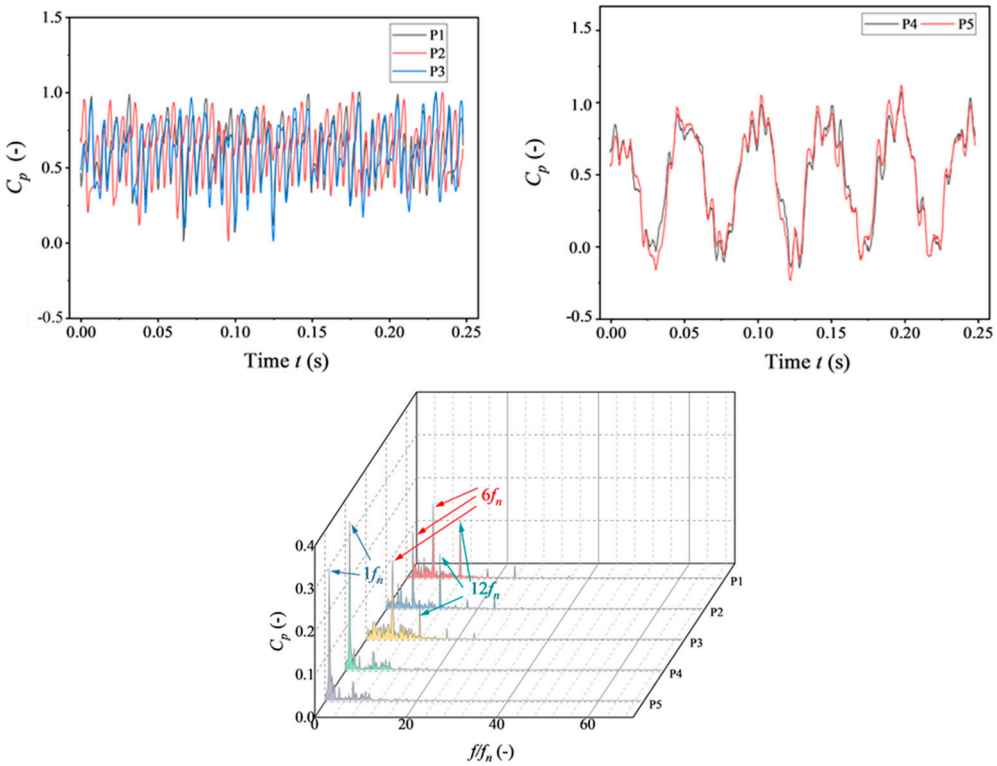

Figure 10. 6+6 Blade Pressure pulsation time-frequency domain diagram.

Based on the spectral results from the P4 and P5 measurement points, further analysis can be conducted on the potential impact of the flow in the draft tube on the hydraulic imbalance of the runner. Under partial load conditions, the spiral vortex band in the draft tube will generate a circumferential non-uniform pressure field. This disturbance will

propagate upstream and act on the runner, thereby causing a hydraulic radial imbalance. The rotational frequency f_n is an important characteristic frequency of the hydraulic imbalance. This study only used discrete measurement points to collect pressure signals and did not perform integral calculations on the pressure of the entire circumferential wall of the runner. Therefore, it is impossible to provide a quantitative numerical value for the hydraulic imbalance force. From a qualitative perspective, the 6+6 scheme has suppressed the occasional large low-frequency pressure pulsations in the draft tube, which is helpful in reducing the circumferential pressure inhomogeneity caused by the vortex band and has the potential to alleviate the hydraulic imbalance; however, this configuration also changes the spectral composition of the bladeless area and the frequency-related excitation components also change. This effect may bring new imbalance risks, and this effect needs to be further quantitatively verified through integral calculation of the runner wall pressure in the future.

Spectra for the two runner configurations are obtained using different normalization references. Therefore, spectral-peak heights shown in Figures 9 and 10 cannot be directly applied for quantitative inter-case comparison; peak-to-peak coefficients in Table 4 are adopted for quantitative evaluation. Therefore, the calculation is as follows, as shown in Equation (6):

$$C_p = \frac{p - p_{avg}}{\rho g H} \times 100\% \quad (6)$$

where C_p represents the intensity of pressure pulsation, p is the absolute pressure at a certain measurement point at a specific moment, and p_{avg} is the average pressure over time under this steady-state operating condition.

Table 4. The comparison results of pressure pulsation peak-to-peak values between the 9 Blade and the 6+6 Blade runner.

Measurement Points	9 Blade	6+6 Blade	Change
P1	16.916%	16.941%	+0.15%
P2	17.572%	17.955%	+2.18%
P3	4.008%	3.985%	−0.56%
P4	1.675%	1.248%	−25.52%
P5	1.729%	1.386%	−19.83%

The statistical results of peak-to-peak pressure fluctuations at each measurement point for the two sets of rotors are shown in Table 4, and the comparison in the form of columns is presented in Figure 11. The peak-to-peak values at the measurement point P1 in the vaneless area remain basically stable, while those at P2 increase slightly by 2.18%. P3 remains basically unchanged. The average peak-to-peak coefficient of the three measurement points in the vaneless area increases from 12.832% to 12.960%, and the fluctuation amplitude at some local measurement points deteriorates slightly. In contrast, the measurement points in the draft tube area show a decrease of 25.52% and 19.83% for P4 and P5 respectively. When the time-domain signals are statistically analyzed on a cycle-by-cycle basis, it can be found that the 6+6 scheme does not uniformly reduce the fluctuation level of each rotational cycle. Its main function is to suppress the occasional large pressure fluctuations in the prototype scheme and improve the periodic consistency of the pressure fluctuation signal.

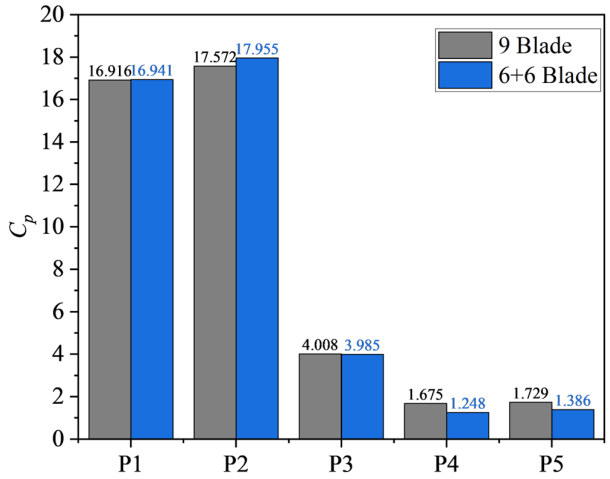

Figure 11. Comparison of pressure pulsation peak-to-peak values for the 9-blade and 6+6-blade configurations.

5. Conclusions

This paper establishes a CFD simulation model of the high-head reversible pump-turbine full-flow channel adopting the SST *k*-*ω* turbulence model. The external operating characteristics of the pump are validated against model test data, Guided by the engineering development concept of prioritizing pump operating conditions and verifying performance via turbine operating conditions, this study systematically compares the hydraulic performance, steady flow field distribution, and unsteady pressure pulsation characteristics between two runner designs: the conventional 9-blade configuration and the novel 6+6 long-short blade configuration. The key research conclusions, together with the technological novelty and comparative performance evaluation of the two designs, are summarized as follows:

(1) Under the pump mode, the 6+6 long-short blade design effectively shifts the hump-instability range of the pump-turbine toward a lower flow rate, isolating the unstable operating region from the conventional normal operating range of the unit. The arranged short blades partition the internal flow channel, which significantly suppresses the generation of large-scale blade passage vortices under crest conditions and mitigates the asymmetric flow distribution in the vaneless area. Nevertheless, this novel configuration also introduces inherent performance compromises: the junction interface between long and short blades induces local secondary flow and flow impact losses, leading to a steeper head drop under high-flow operating conditions, and the leading edge of short blades faces potential cavitation risks. Notably, the 6+6 long-short blade structure only realizes the offset of hump instability rather than complete elimination of the crest phenomenon. Unsteady flow analysis further demonstrates that the long-short blade layout modulates the pressure pulsation spectrum in the vaneless area, and its flow optimization effect exhibits prominent operating condition dependence.

(2) Under the 50% partial load turbine mode, the two runner designs present distinct differentiated performance advantages. The novel 6+6 long-short blade configuration delivers remarkable improvements in turbine draft tube flow stability, which can effectively reduce the peak-to-peak pressure fluctuation amplitude in the draft tube, suppress sporadic extreme large pressure fluctuations, and enhance the periodic consistency of internal flow fluctuations. In contrast, the conventional 9-blade runner shows more stable pressure pulsation performance in the vaneless area with no abnormal amplitude increment. The 6+6 long-short blade design fails to optimize

vaneless area pressure pulsation, and even causes a slight increase in fluctuation amplitude at partial measurement points, revealing a typical performance trade-off characteristic. This indicates that the flow optimization benefits of the long-short blade configuration are localized, and it cannot achieve full-area pressure pulsation suppression for turbine operating conditions; neither of the two designs can realize comprehensive hydraulic stability optimization across all flow regions.

(3) Technically, this study fills the existing research gap in the multi-condition comparative performance analysis of long-short blade runners for high-head reversible pump-turbines. Most previous studies only focused on the pump hump characteristic improvement of long-short blade designs while ignoring the coupled turbine-side flow stability and multi-working-condition adaptability, and this work provides a targeted technical supplement for the optimal design of high-head pumped storage units. In terms of design application, the performance evaluation of the two runner blade designs proves that for 655-m-level high-head reversible pumped storage turbines, single-objective optimization of pump hump characteristics is insufficient and one-sided. The optimized 6+6 long-short blade design is more suitable for engineering scenarios with strict requirements on pump operating stability and low-flow hump instability suppression, while the conventional 9-blade design is more applicable for units prioritizing vaneless area flow stability and uniform full-condition performance.

Author Contributions: Conceptualization, K.Z. and X.Z.; methodology, Y.L.; software, J.L.; validation, W.X. and R.X.; formal analysis, J.L.; investigation, X.Z.; resources, X.Z.; data curation, K.Z.; writing—original draft preparation, R.X.; writing—review and editing, J.L.; visualization, Y.L.; supervision, Y.L.; project administration, W.X.; funding acquisition, All authors have read and agreed to the published version of the manuscript.

Funding: This research was funded by State Grid XinYuan Group Co., Ltd. Science and Technology Project (SGXYKJ-2025-038).

Data Availability Statement: The datasets generated during and/or analyzed during the current study are available on request from the corresponding author.

Conflicts of Interest: Author Kai Zheng was employed by the company State Grid Xinyuan Group Co., Ltd.; Author Xijun Zhou and Wei Xiao were employed by the company Pumped Storage Technology and Economy Research Institute of State Grid Xinyuan Company Ltd.; Author Yaopeng Li was employed by the company Jilin Dunhua Pumped Storage Co. The authors declare that this study received funding from State Grid XinYuan Group Co., Ltd Science and Technology Project (SGXYKJ-2025-038). The funder was not involved in the study design, collection, analysis, interpretation of data, the writing of this article or the decision to submit it for publication.

References

1. Huang, R.; Wang, P.; Zhang, S.F. Experiences and lessons for China's energy transition: From the fire wood era to the low carbon era. *Energy Sustain. Dev.* **2024**, *78*, 101368. [CrossRef]
2. Kan, K.; Yu, Y.; Zhou, Y.; Chen, Y.; Ye, C. Numerical investigation of multiscale flow-induced vibration and fatigue life prediction of a large Francis turbine. *Energy* **2025**, *335*, 138334. [CrossRef]
3. Ren, C.; Ren, Q.; Gao, X. Research on low-carbon electric power development in China under "carbon neutralization and carbon peak" background. *Therm. Power Gener.* **2024**, *53*, 1–7.
4. Al Khaffaf, I.; Tamimi, A.; Ahmed, V. Pathways to carbon neutrality: A review of strategies and technologies across sectors. *Energies* **2024**, *17*, 6129. [CrossRef]
5. Lu, Y.; Liu, Z.; Zhao, Y.; Wang, Z.; Presas, A. Study on evolution characteristics of energy dissipation and vortex in pump-turbine during load rejection transition process. *Phys. Fluids* **2025**, *37*, 025104. [CrossRef]
6. Rehman, S.; Al-Hadhrami, L.M.; Alam, M.M. Pumped hydro energy storage system: A technological review. *Renew. Sustain. Energy Rev.* **2015**, *44*, 586–598. [CrossRef]

7. Liang, A.; Chang, Y.; Zhang, W.; Yao, Z.; Zhu, B.; Wang, F. Research on the evolution law and energy loss characteristics of rotating stall in a pump-turbine under pump mode. *Energy* **2025**, *330*, 136696. [CrossRef]
8. Presas, A.; Valentin, D.; Zhao, W.; Egusquiza, M.; Valero, C.; Egusquiza, E. On the use of neural networks for dynamic stress prediction in Francis turbines by means of stationary sensors. *Renew. Energy* **2021**, *170*, 652–660. [CrossRef]
9. Hoffstaedt, J.; Laguna, A.J.; Ruiz, R.A.; Schürenkamp, D.; Goseberg, N.; Truijen, D.; De Kooning, J.; Stockman, K.; Fahlbeck, J.; Nilsson, H. Analysis of a contra-rotating pump-turbine for low-head applications: An experimental study and numerical comparison. *Energy Convers. Manag.* **2025**, *341*, 119950. [CrossRef]
10. Zheng, Y.; Tang, K.; Xu, L.; Ren, S.; Xu, J.; Wang, Y.; An, D.; Ye, C. Stability Analysis of Pump-Turbine in Hump Zone Based on Omega Vortex Identification Method. *Water* **2024**, *16*, 3443. [CrossRef]
11. Zheng, K.; Chen, L.; Ren, S.; Xiao, W.; Xiao, Y.; Rai, A.K.; Shi, G.; Hao, Z. Pressure Fluctuation Characteristics of a Pump-Turbine in the Hump Area under Different Flow Conditions. *J. Mar. Sci. Eng.* **2024**, *12*, 1654. [CrossRef]
12. Yang, J.; Cheng, X.; Liu, X.; Feng, X.; Pan, K. Influence mechanism of impeller internal flow structure in the pump-mode hump instability of pump turbine: A compressible flow solution. *J. Energy Storage* **2024**, *92*, 112049. [CrossRef]
13. Li, Y.; Hao, P.; Zhang, Z.; Zhang, L.; Hai, H.; Zhang, H.; Wang, X.; Wang, J.; Zhao, Z.; Peng, P. Characterization of Pressure Pulsation Propagation in a Pump-Turbine Based on the Same-Frequency Tracking Method. *Energy Sci. Eng.* **2025**, *13*, 3588–3604. [CrossRef]
14. Gad, M.; Gao, B.; Zhang, N.; Ni, D. Pressure fluctuations in a pump as turbine with splitter blades: A comparative study of pump and turbine modes. *J. Energy Storage* **2026**, *165*, 122351. [CrossRef]
15. Yang, Z.; Cao, C.; Fang, J.; Zhang, B.; Li, C.; Hou, X. Mechanism of Pressure Fluctuations and Flow Patterns Under Steady Operating Conditions of a Variable Speed Pump-Turbine. *Processes* **2025**, *13*, 3511. [CrossRef]
16. Liu, B.; Luo, Y.; Jin, F.; Zhang, H.; Ouyang, J.; Wang, Z.; Ma, M. Effect of runner blades-guide vanes combination on a prototype pump-turbine pressure pulsation characteristics in turbine mode with special emphasis on rotor-stator interaction. *Phys. Fluids* **2025**, *37*, 096111. [CrossRef]
17. He, W.; Luo, Z.; Guo, T.; Han, J. Numerical investigation of energy dissipation and vortex characteristics of a pump-turbine with splitter blades under the influence of rotating stall in the hump region. *Phys. Fluids* **2025**, *37*, 095155. [CrossRef]
18. Wei, X.-Y.; Kang, X.-F.; Pei, J.; Wang, W.-Q. Sediment erosion of Francis turbine with splitter blades. *Int. J. Mech. Sci.* **2025**, *304*, 110674. [CrossRef]
19. Lu, J.; Li, F.; Tao, R.; Yao, Z.; Xiao, R.; Liang, Q.; Liu, W. Nonlinear stability analysis of the transient startup process of the turbine mode of pumped storage unit under different control strategies. *Energy Convers. Manag.* **2026**, *359*, 121546. [CrossRef]
20. Lu, J.; Tang, Y.; Tao, R.; Zhu, D.; Yao, Z.; Xiao, R.; Wang, F.; Liang, Q.; Liu, W. Research on the dynamic evolution law of the transient process of pump mode shutdown in pump-turbine. *J. Energy Storage* **2026**, *156*, 121615. [CrossRef]
21. Lu, J.; Tao, R.; Yao, Z.; Xiao, R.; Liu, W. Transient simulation energy study of fast opening of guide vane during start-up of pump turbine in energy storage mode. *Energy* **2025**, *324*, 135964. [CrossRef]
22. Lu, J.; Han, X.; Tao, R.; Xiao, R.; Liang, Q. Research on transient performance changes during the non-simultaneous opening process of guide vanes in reversible pump-turbine units in pump mode. *Energy* **2025**, *335*, 138331. [CrossRef]
23. Li, X.L.; Dong, H.Y.; Lu, Y.G.; Li, X.J.; Wang, Z.W. Study on Transient Flow Characteristics of Pump Turbines during No-Load Condition in Turbine Mode Startup. *Water* **2024**, *16*, 2741. [CrossRef]

Disclaimer/Publisher's Note: The statements, opinions and data contained in all publications are solely those of the individual author(s) and contributor(s) and not of MDPI and/or the editor(s). MDPI and/or the editor(s) disclaim responsibility for any injury to people or property resulting from any ideas, methods, instructions or products referred to in the content.